 https://doi.org/10.18171/1.094104

Seismic monitoring of the October 2023 storm surge along the coast of the Baltic Sea

Lars Wiesenberg[1], Christian Weidle[2], Knut Krämer[2], Christoph Pilger[3], Christian Winter[2] and Thomas Meier[2]

[1] Institute of Geoscience, Christian-Albrechts-University Kiel, Kiel, Germany; lars.wiesenberg@ifg.uni-kiel.de
[2] Institute of Geoscience, Christian-Albrechts-University Kiel, Kiel,
[3] Federal Institute for Geosciences and Natural Resources, Hanover, Germany

Summary

The coupling between ocean and seismic waves – often referred to as (oceanic) microseism – is a well-established concept since the 1950's. Ocean and seismic waves are correlating not only on seasonal to annual, but also on daily timescales, in particular during extreme weather events. The most prominent microseism signals have periods below ten seconds and originate from interfering water waves. They are called secondary microseism and can be related to marine storm activity. While some secondary microseism may arrive from far-away coastal regions, a strong contribution also results from nearby coastal wave activity. This paper shows that measurements of microseism from our recently expended seismic network in northern Germany are well suited to monitor wave propagation processes in coastal areas during extreme weather events like the October 2023 storm surge. We utilize three component seismic data from seven stations along the German Baltic Sea coastline and infrasound data from the local array Kühlungsborn (IKUDE) to investigate secondary microseism and atmospheric pressure variations during the storm surge. Spectral investigations over time show distinct local differences in secondary microseism of the Baltic Sea at three different near coastal sites which correlate with half the peak wave period in each respective area. Infrasound measurements reveal additional noise sources, such as nearby wind parks, anthropogenic sources or microbaroms in the North Atlantic and probably the North Sea which are transferred through the atmosphere and absent in seismic data and vice versa. Therefore, sources of our seismic measurements during the October 2023 storm surge are related rather to ocean generated microseism, transferred through the solid Earth than to atmospheric pressure sources. As amplitudes related to secondary microseism of the Baltic Sea decrease with increasing distance of the station to the coast, this allows for an estimation of a sensitivity range along the Baltic Sea coastline. For seismic monitoring of coastal areas, seismic stations are needed to be within 25−30 km distance to the coastline to precisely detect locally generated microseism.

Keywords

storm surge, Baltic Sea, seismic monitoring, ocean generated microseism, infrasound

Received 26. September 2024, reviewed 30. September 2024, revised 20. December 2024, accepted 21. December 2024, available online 27. January 2025.

Zusammenfassung

Seismische Wellen, die durch die Interaktion von Ozeanwellen mit dem Meeresboden erzeugt werden, bezeichnet man als Meeresmikroseimik. Erste Untersuchungen gehen auf die 1950er Jahre zurück. Ozeanwellen und seismische Wellen korrelieren nicht nur auf saisonaler oder jährlicher Skala, sondern auch auf täglichen Zeitskalen, insbesondere während Extremwetterereignissen. Die stärksten Signale werden bei Perioden kleiner als zehn Sekunden erzeugt und entstehen durch turbulente Wellenbewegung. Sie werden als sekundäre Meeresmikroseismik bezeichnet und häufig mit maritimer Sturmaktivität in Verbindung gebracht. Sekundäre Meeresmikroseismik kann im offenen Ozean durch interferierende Wellen oder in Küstennähe entstehen. In dieser Arbeit zeigen wir, dass unser erweitertes Netzwerk an seismischen Stationen in Norddeutschland geeignet ist, um lokale Wasserwellenbewegung in Küstennähe während Extremwetterereignissen, wie z. B. der Ostseesturmflut im Oktober 2023 mittels Meeresmikroseismik zu überwachen. Dazu benutzen wir Daten von sieben 3-Komponenten Breitbandseismometern an verschiedenen Standorten der deutschen Ostseeküste, sowie Daten von Infraschallstationen in Kühlungsborn (IKUDE) um sekundäre Meeresmikroseismik und atmosphärische Druckschwankungen während der Sturmflut zu untersuchen. Die seismischen Daten zeigen deutliche Unterschiede bei Signalen im Periodenbereich sekundärer Meeresmikroseismik an drei küstennahen Standorten entlang der Ostseeküste. Diese korrelieren mit der halben maximalen Wellenperiode, die lokal an den jeweiligen Standorten in unmittelbarer Küstennähe gemessen wurde. Die Infraschall-Daten zeigen zusätzliche Rauschquellen, wie z. B. durch nahegelegene Windparks, anthropogene Einflüsse oder Mikrobarome aus dem Nordatlantik und möglicherweise aus der Nordsee, die über die Atmosphäre übertragen und nicht in den seismischen Daten erkennbar sind und umgekehrt. Dementsprechend können wir die seismischen Signale, die während der Ostseesturmflut im Oktober 2023 gemessen wurden auf Meeresmikroseismik, die über die feste Erde und nicht über die Atmosphäre übertragen wurden, zurückführen. Die gemessenen Amplituden sekundärer Meeresmikroseismik der Ostsee nimmt zudem mit zunehmender Entfernung zur Küste ab. Diese Abnahme können wir nutzen, um einen Einflussbereich zu bestimmen, in welchem lokal generierte Meeresmikroseismik erzeugt wird. Um eine seismische Überwachung von Küstengebieten in der Ostsee zu gewährleisten und Meeresmikroseismik zu messen, sollten Seismometer keine größere Entfernung als 25 bis 30 km zur Küste besitzen.

Schlagwörter

Sturmflut, Ostsee, Seismische Überwachung, Meeresmikroseismik, Infraschall

1 Introduction

From 19th to 21st October, 2023, an exceptional storm surge in the western Baltic Sea affected many parts of the German and Danish coastal areas. The storm was driven by easterly winds resulting from the difference in air pressure between a high-pressure system over Scandinavia and a low-pressure system over the British Isles. While the water was pushed away from the coasts of the North Sea, a severe storm surge affected the western Baltic Sea coast lines. Maximum (sustained) wind speeds of 33 m/s (10 Bft) were measured in Flensburg. Already on the day before the actual storm surge, high wind speeds of 9−10 Bft were measured at the sites of Kiel and Kap Arkona/Rügen (Figure 1a). Both measuring stations stopped operating due to the storm surge in the evening of 20th October (Figure 1a). The storm surge affected mostly the coastal areas of Schleswig Holstein and southern Denmark, where it led to flooding in major cities like Flensburg, Schleswig and Eckernförde. Peak sea

levels of 2.27 m above average were reached in Flensburg, whereas maximum values of 1.95 m above average were measured in the Bay of Kiel and 1.63 m above average in the Bay of Mecklenburg (Figure 1b) (BSH 2024). The water levels in the Bays of Kiel- and Lübeck were already up to 50 cm above average sea level days before the storm surge (BSH 2024).

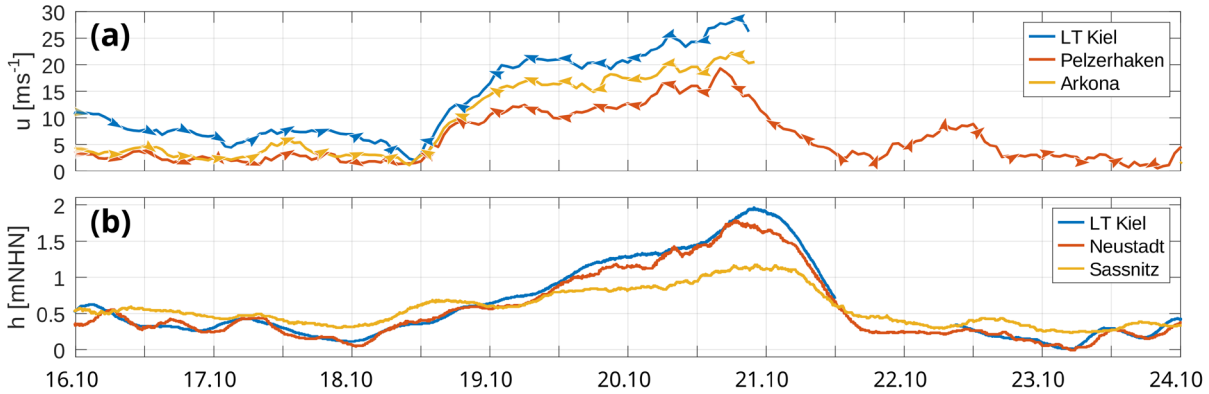

Figure 1: Wind speed and -direction (a) and sea level elevation (b) during the time of the October 2023 storm surge at the lighthouse Kiel (LT Kiel), Pelzerhaken and Neustadt in the Bay of Lübeck and on the island of Rügen (Arkona, Sassnitz). Datasets are obtained from the Federal Waterways and Shipping Agency (WSV) and the German Weather Service (DWD). For more information see data availability statement.

Due to enhanced wind speeds and ocean wave parameters such as significant wave height and peak wave period, the October 2023 storm surge provides an opportunity to investigate seismic waves that are locally generated in the Baltic Sea and vary along the German coast lines. These seismic waves are called ocean generated microseism. In this contribution, we introduce the recently expanded permanent seismic network in Schleswig Holstein and Mecklenburg-Western Pomerania and demonstrate its potential for local microseism monitoring. Continuous seismic data from stations in coastal regions will be analyzed for spectral variations over time. By covering a broad period range, our findings are not limited to microseism in the Baltic Sea, but will also show imprints from other seas and oceans, such as the North Sea and the North Atlantic. We validate the robustness of our seismic observations by comparing them with measurements of acoustic waves in the atmosphere – so called infrasound and demonstrate the advantages and benefits of the permanent seismic network along the German coastal area of the Baltic Sea.

1.1 Microseism

The spectrum of global ambient seismic noise is dominated by two peaks at periods between 1–30 s. In general, they originate from the interaction of sea surface waves with the solid Earth at the sea floor and are referred to as ocean generated microseism. The first peak, called primary microseism, has its maximum at periods of 14−16 s, which is the same period as surface gravity waves in the North Atlantic. The second peak is typically larger in amplitude than the first one and is centred at a period of around 7−10 s which is half the period of surface gravity waves and therefore called secondary microseism. Ocean microseism was already observed more than 100 years ago (e.g. Bertelli 1872, Omori 1899, Wiechert 1904). However, while a general connection between storm activity and ocean

generated microseism was quickly established (Wiechert 1904, Zöppritz 1908) and seismic recordings were even used to forecast the arrival of storm systems in the North Atlantic (Deacon 1947) or the Indian Ocean (Davy et al. 2014), the details of microseism generation (e.g. sea surface wave fields, water currents, wind speed, bathymetry or lithology) are still not completely understood. Contemporary investigations of microseism range from global scale in ocean basins (Essen et al. 2003, Ardhuin et al. 2011, Ardhuin et al. 2012, Ardhuin et al. 2016) to local scales in marginal seas, such as the North Sea and Baltic Sea (Becker et al. 2020, Lepore and Grad 2018), investigations of local storm events, e.g. in the Mediterranean Sea (e.g. Ferretti et al. 2018, Cutroneo et al. 2021) or source locations of ocean generated microseism (Moschella et al. 2020).

Primary microseism is caused by shoaling of ocean waves (Ardhuin et al. 2015) and its generation region is therefore usually in near coastal areas or shallow water regions. The amplitudes are distinctly smaller than those of secondary microseism. However, due to their large wavelength, they are globally measurable. Secondary microseism is caused by superposition of ocean waves of nearly opposing directions and equal frequency (e.g. Longuet-Higgins 1950, Ardhuin et al. 2015) which causes pressure fluctuations in the water column. Source regions of secondary microseism are near coastal regions due to reflections of incoming ocean waves at the shore (e.g. Bromirski and Duennebier 2002) and in open (deep) water locations (Longuet-Higgins 1950). Due to their different generation mechanisms, primary microseism has a larger horizontal component of displacement, whereas secondary microseism is dominant on the vertical component (Juretzek and Hadziioannou 2016). Ocean wave periods are mainly controlled by wind speed and the fetch length, the length of uniform wind direction, not limited by land masses (Bretschneider 1959, Pierson Jr and Moskowitz 1964). Periods are generally lower in marginal seas like the North Sea or Baltic Sea due to their lower fetch length. Reference values of dominant periods for the North Sea are 8−10 s for primary microseism and 4−5 s for secondary microseism (e.g. Becker et al. 2020). In the Baltic Sea, dominant periods of microseism are even lower, ranging between 5−6 s for primary and < 3 s for secondary microseism (e.g. Lepore and Grad 2018). Moreover, microseism generation varies spatially on local scale in coastal regions, depending on different source mechanisms or structural influences (e.g. Juretzek and Hadziioannou 2016).

1.2 Network and Datasets

Northern Germany is in general a rather weak seismicity region with low level of exposure to seismic hazard. Therefore, seismic monitoring had low priorities in the past. However, low to moderate magnitude earthquakes occasionally occur in the North German Basin. The main reasons for natural seismic events are post glacial relaxation, salt tectonics and NE-SW directed compressional stresses in the vicinity of the Trans-European-Suture-Zone (e.g. Leydecker 2011). In cooperation with the Federal Institute for Geosciences and Natural Resources (BGR), the Geological Survey of Schleswig-Holstein (LfU SH), the Geological Survey of Mecklenburg Western Pomerania (LUNG M-V) and the German Research Centre for Geosciences (GFZ), the number of permanent broadband stations in the North German Federal States of Schleswig Holstein and Mecklenburg Western Pomerania was increased from formerly four stations in 2013 to currently 16 (Figure 2a; e.g. Stammler et al. 2021). The regional network is supplemented by dense local seismic networks in focus

areas, such as the salt dome in Bad Segeberg (Figure 2c) or in marginal seas on the islands of Heligoland (Figure 2b) and Rügen (Figure 2e). In total, continuous seismic waveform data are collected in realtime from currently 35 seismic stations. Besides natural seismicity, other local seismic events relate to explosions (e.g. Navy exercises, cleaning of unexploded ordnance or the explosion of the Nord Stream pipelines in 2022), as well as subrosion and rockfall events in coastal areas (e.g. Leydecker 2011). Continuous passive seismic measurements can be used not only for event monitoring, but also for monitoring of ocean generated microseism or long period seismic noise (> 20 s periods), often referred to as infragravity waves (e.g. Webb 1998, Webb and Crawford 2010). Investigations of ocean generated microseism and infragravity waves are supported by offshore monitoring of surface gravity waves and ocean currents in the North Sea and Baltic Sea via buoys and platforms. They are operated by the Federal Maritime and Hydrographic Agency (BSH, blue dots in Figure 2a) in German waters. Moreover, a local infrasound Array in Kühlungsborn (IKUDE, Figure 2d), operated by the BGR since July 2021, provides complementary information on atmospheric pressure variations. It consists of four individual infrasound sites, each one equipped with one MB3d microbarometer and a wind reduction system (WNRS). The WNRS consists of 24 equally-long hoses with an air inlet port on each end in a circled area of 12 m diameter. The IKUDE infrasound array is collocated with a broadband seismic station (KBON, Figure 2d). Information on the access to all used datasets are written in the data availability statement.

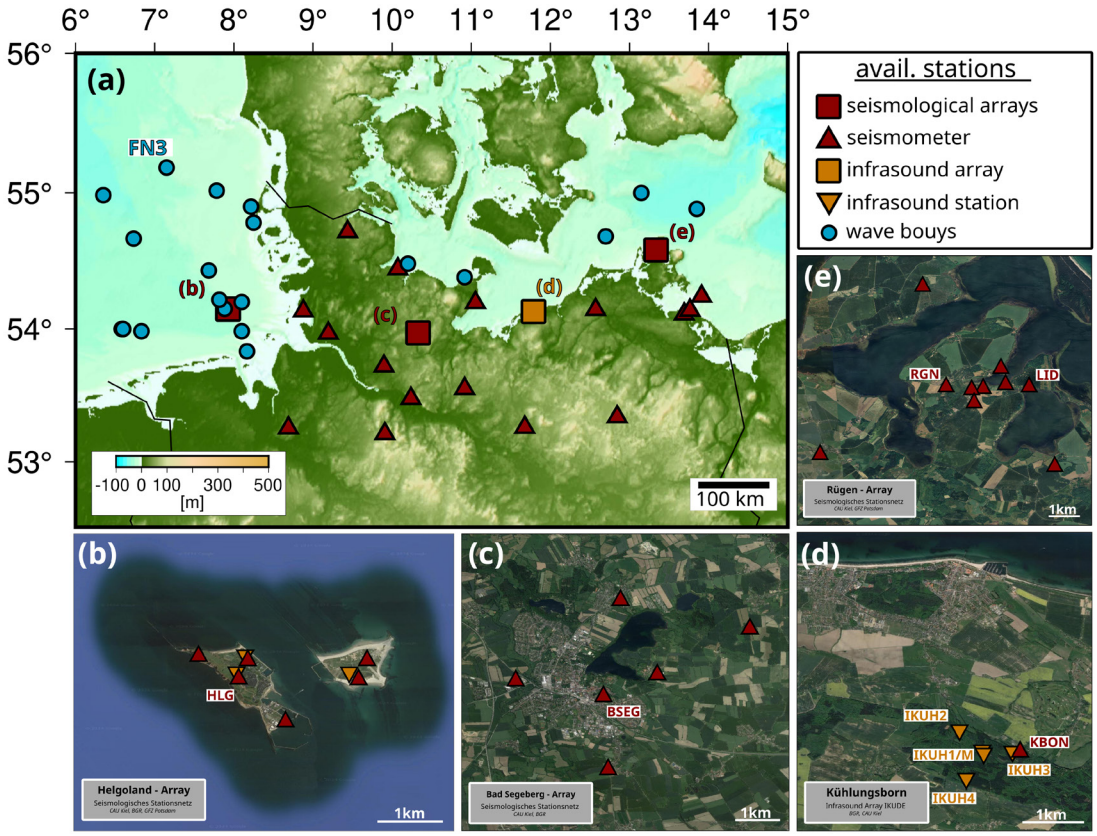

Figure 2: Multidisciplinary network in the German coastal areas of the North Sea and Baltic Sea (a). Red triangles indicate the location of the permanent seismic broadband stations, whereas orange triangles show the location of infrasound stations. Offshore buoys are marked as blue dots. Local seismic and infrasound arrays are shown as red/orange squares, with close-ups of the Heligoland seismic array (b), the Bad Segeberg seismic array (c), the infrasound array IKUDE in Kühlungsborn (d) and the Rügen seismic array (e).

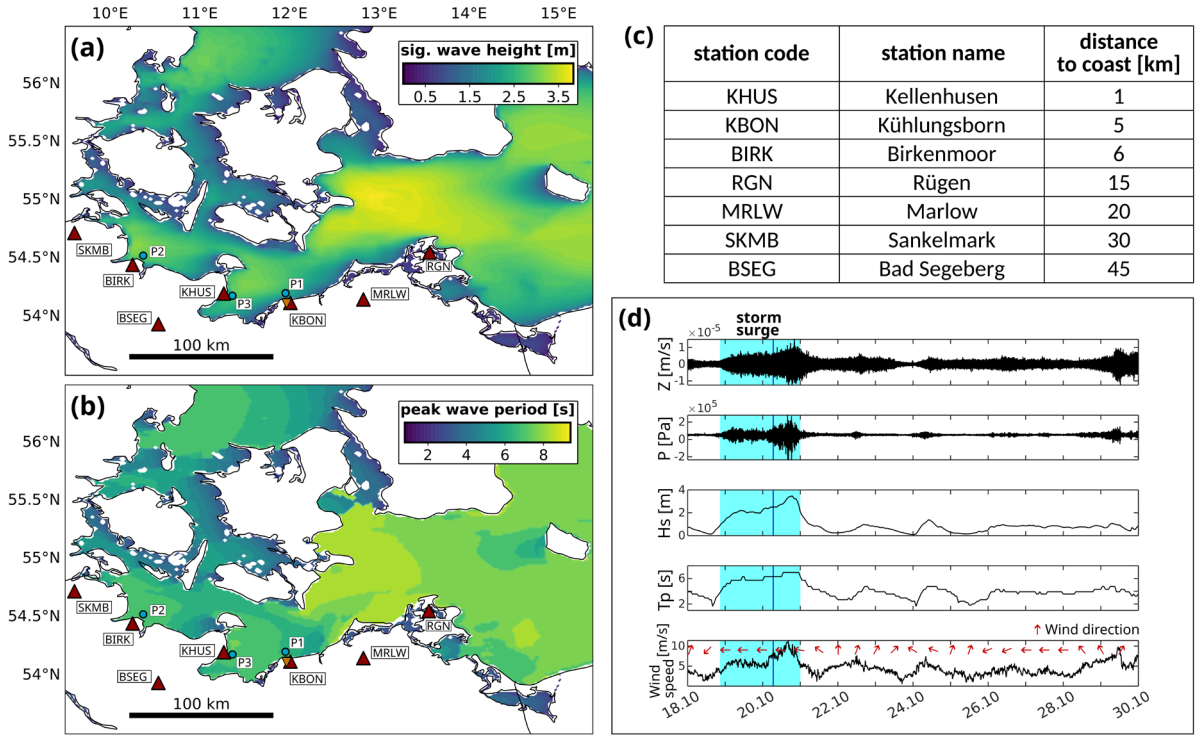

station code	station name	distance to coast [km]
KHUS	Kellenhusen	1
KBON	Kühlungsborn	5
BIRK	Birkenmoor	6
RGN	Rügen	15
MRLW	Marlow	20
SKMB	Sankelmark	30
BSEG	Bad Segeberg	45

Figure 3: Overview of the used datasets. Model data of significant wave height and peak wave period on 20th October 2023, 06:00 CET, during the storm surge are shown in (a) and (b), respectively. Seismic stations used in this study are shown as red triangles. Their distances to the coast are summarized in (c). An overview of the entire dataset is exemplary shown for the local array of Kühlungsborn (d). From top to bottom it shows the vertical component seismic data (Z), atmospheric pressure data from the infrasound station IKUH1 (P), significant wave height (H_s) and peak wave period (T_p) at P1 and wind speed and -direction of the nearby weather station in Bastorf-Kägsdorf (orange triangle in (a) and (b)), operated by the German Weather Service (DWD). The time of the storm surge is highlighted in light blue.

For the seismic investigation of the October 2023 storm surge, we utilize three component continuous data from seven sites with variable distances to the German Baltic Sea coastline from 18th to 29th of October (Figure 3a, b, c). Sea surface gravity wave data is provided as numerical model results of the Baltic Sea model by the Norwegian Meteorological Institute via the Copernicus Marine Service (see data availability statement for access information). The model output has a spatial resolution of 3*x*3 km and a temporal resolution of one hour, exemplary shown in Figure 3 for the 20th of October, 06:00 CET during the storm surge with significant wave height (H_s) as well as peak wave period (T_p). For comparing local seismic variations at near coastal stations and variations in surface gravity waves, three locations (P1-P3 in Figure 3a and b) are selected. In addition, surface gravity wave data from the FINO3 platform in the North Sea (FN3 in Figure 2a) is utilized. Figure 3d shows a compilation of the multidisciplinary dataset in Kühlungsborn. Raw infrasound data is shown exemplary from IKUH1 (for exact location see Figure 2d). Significant wave height and peak wave period are obtained from P1. Wind speed and -direction, with a temporal resolution of ten minutes are obtained from the nearby weather station of the German Weather Service (DWD) in Bastorf-Kägsdorf (orange triangle in Figure 3a and b; see data availability statement for access information). All parameters show increasing amplitudes during the storm surge, while the wind direction was overall from the East. After the storm surge, wind direction changed to southerly directions until the 25th October. During that

time, amplitude variations in peak wave period and significant wave height are accompanied by similar variations in amplitude of the vertical seismic component and Infrasound.

2 Seismic observations during the storm surge

Raw continuous three component seismic data was utilized to evaluate the variation of spectral content over time and to compare our measurements to the varying ocean generated microseism. Waveforms are cut into segments of 15 min and amplitude spectra calculated for each segment and each component in a period range of 0.125−250 s. The horizontal component (H) is calculated using the Euclidean norm of the amplitude spectra of the North (N) and East (E) component: $H = \sqrt{N^2 + E^2}$. Figure 4a shows a histogram representation of the vertical component spectra over all 15 min segments and all days at the site of Kühlungsborn. Ocean generated microseism is dominant at periods of ≈1−30 s, where the ambient seismic noise field has the largest amplitudes. This is valid for all stations used in this study (Figure S1 in the supplemental material).

When displayed over time, the vertical component spectrogram (Figure 4b) reveals a large number of distinct signals at different periods. Occasionally occurring strong amplitudes at periods larger than 10 s relate to large earthquakes, whereas amplitude variations at lowest periods can be associated with anthropogenic noise (day-night-rhythm). These observations are consistent at every station (Figure 5) and of no further relevance in this work.

During the October 2023 storm surge, maximum amplitudes in the spectrum are measured at the site of Kühlungsborn (Figure 4b) and the largest spectral variations over time occur at periods between 1 and 3 s. These variations correlate with half the peak wave period of ocean waves at location P1 (white dashed line; for exact location see Figure 3a). Following the definition of primary and secondary microseism (section 1), we therefore associate these amplitude variations with secondary microseism of the Baltic Sea. The spectra at stations Birkenmoor and Kellenhusen (Figure 5a and b), which are of similar or closer distance to the coast as the site of Kühlungsborn (see Figure 3c) show similarly amplitude variations that fit with the half peak wave period in close distance offshore their respective coast (P2 and P3 in Figure 3a and b). A strong visual correlation between the three stations and half peak wave period at all three local points remains even few days after the storm surge ceased. During the 22nd and 23rd October, small seismic amplitudes in the spectrogram of Birkenmoor correlate with small peak wave periods at P2. At the same time, large seismic amplitudes are observable at Kellenhusen and Kühlungsborn which correlate with increased half peak wave periods. At the sites in Marlow (MRLW, Figure 5c) and on the island of Rügen (RGN, Figure 5d), which are 15 to 20 km from the coast, seismic amplitudes are significantly smaller than at near coastal stations, e.g., Kühlungsborn, but still observable over the entire time. At Sankelmark (SKMB, Figure 5e), secondary microseism of the Baltic Sea between 1–3 s period is only observable during the storm surge and on 27th October. Bad Segeberg (BSEG, Figure 5f), which has the largest distance to the Baltic Sea coast of about 50 km, shows no secondary microseism of the Baltic Sea. This indicates that seismic waves of ocean generated microseism in a period range of 1–3 s are locally generated by surface gravity waves in coastal areas of the Baltic Sea. The decrease of seismic amplitudes of secondary microseism of the Baltic Sea with increasing distance to the coast will be further discussed in the next section.

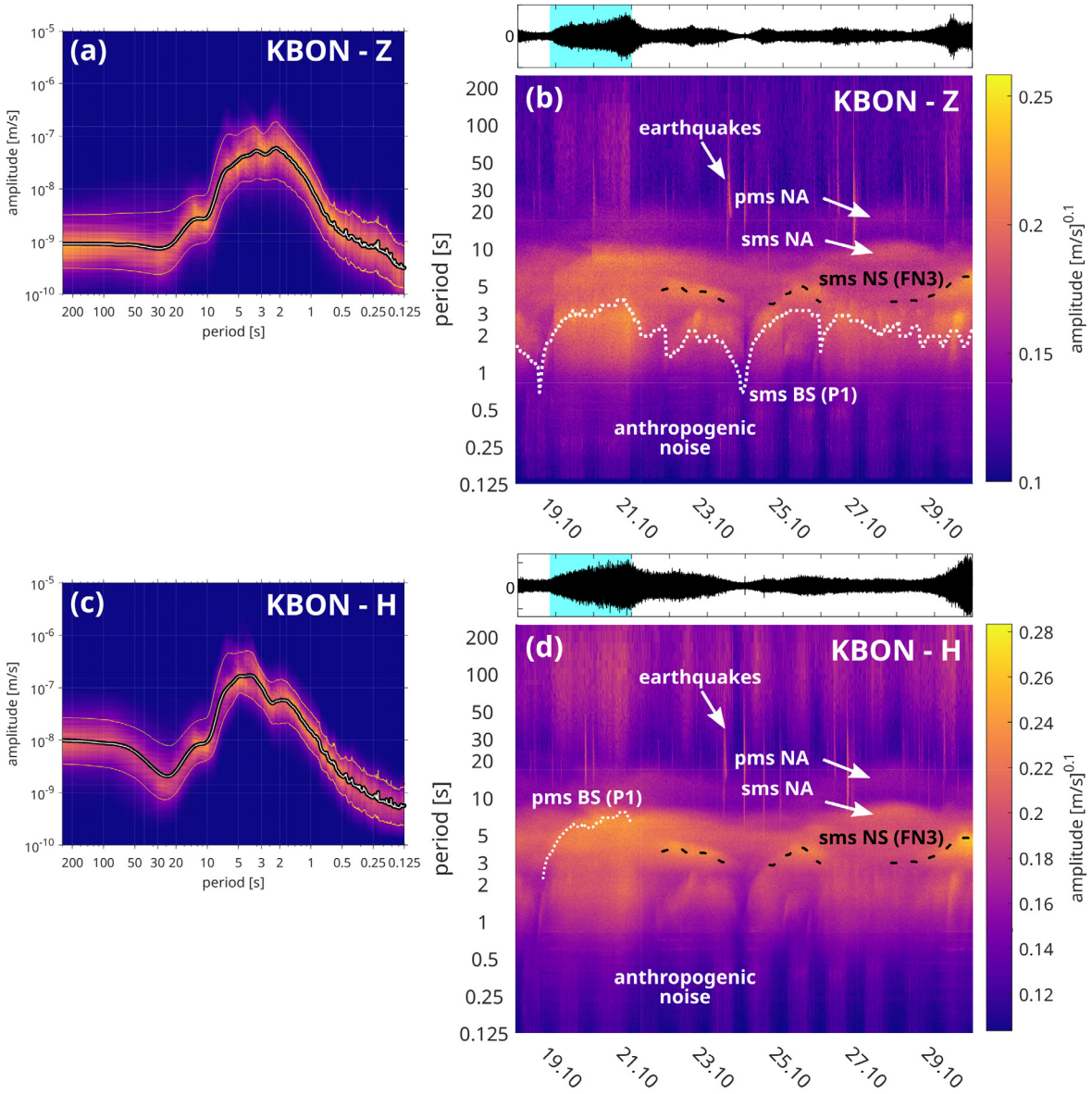

Figure 4: Spectral content of the seismic vertical (a, b) and horizontal (c, d) component at the site of Kühlungsborn. A histogram representation of 15 min spectral amplitude as a function of period is shown in (a) and (c). The median amplitude (white line) and the 10 and 90 percent percentiles (yellow lines) are highlighted. The spectral variations over time (spectrogram) and its raw waveform, filtered between 0.125 and 250 s are shown in (b) and (d). The white dashed line indicates the half peak wave period at location P1 (for exact locations see Figure 3a, b) while the black dashed line shows the half peak wave period measured at the FINO3 platform in the North Sea (for location see Figure 2a). Primary and secondary microseism of the North Atlantic, as well as earthquakes and anthropogenic noise are highlighted. BS: Baltic Sea, NS: North Sea, NA: North Atlantic.

At larger periods (≈5 s), seismic amplitudes at all stations used in this study fit to the half peak wave period measured at the FINO3 platform in the North Sea (black dashed lines in Figure 4b and Figure 5) and therefore can be related to secondary microseism in that region. Largest seismic amplitudes are observed in Sankelmark, the closest station to the North Sea coast. Primary and secondary microseism of the North Atlantic are also visible in all spectrograms (Figure 4b and Figure 5) as well as in the histograms (Figure 4a and Figure S1 in the supplemental material) as they are globally measurable at around 14–16 s and 7–8 s period, respectively.

The horizontal seismic component at Kühlungsborn (Figure 4c and d) shows overall a very similar spectral content compared to the vertical. In detail, larger amplitudes can be observed especially during the storm surge at ≈3–6 s periods both in the histogram as well as the spectrogram. They might reveal primary microseism in the Baltic Sea, which has a larger excitation of the horizontal seismic component. In addition, periods longer than 30 s show higher amplitudes in the horizontal than vertical component over the entire observation interval.

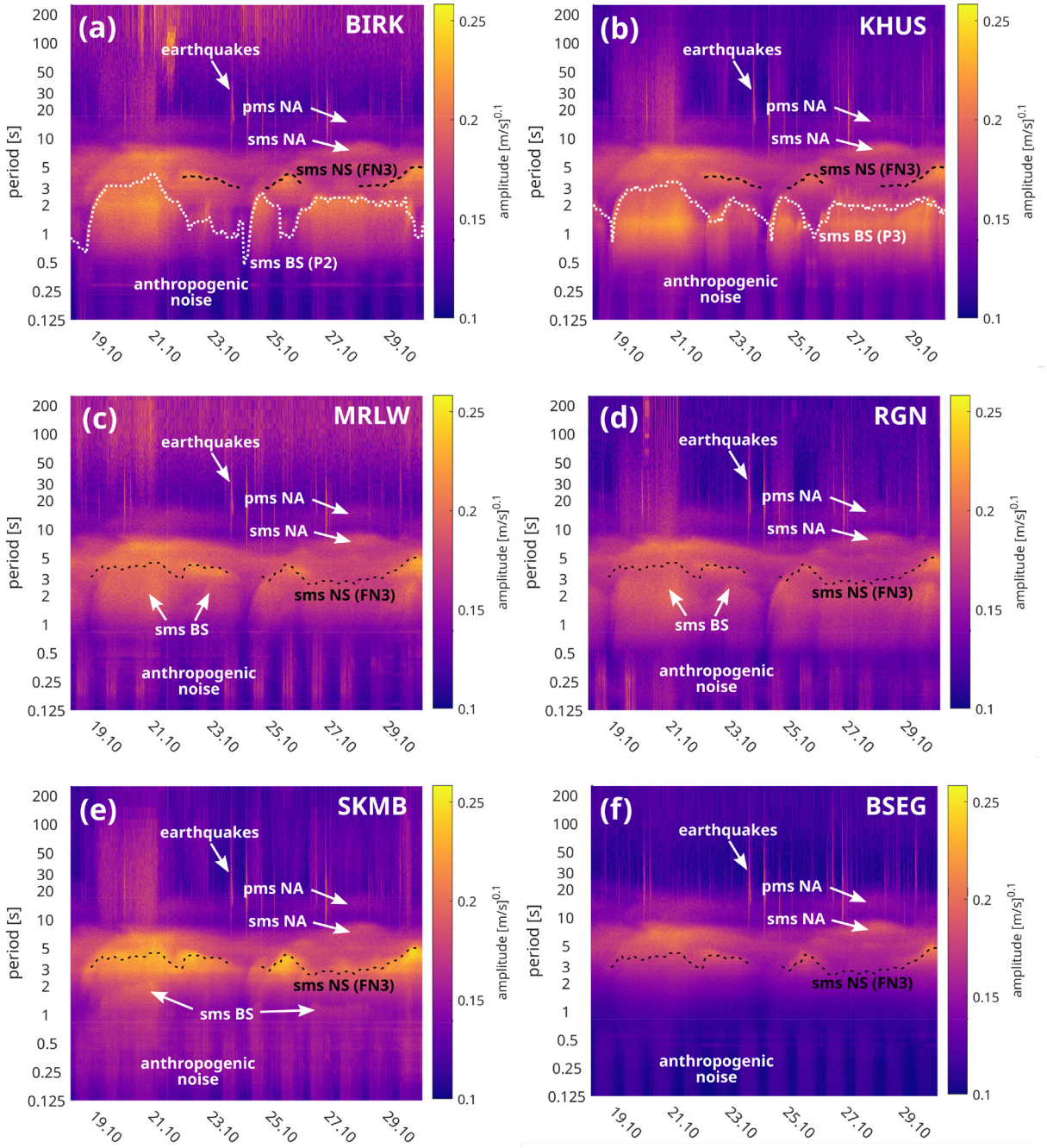

Figure 5: Vertical component seismic spectrograms of stations Birkenmoor (BIRK, (a)), Kellenhusen (KHUS, (b)), Marlow (MRLW, (c)), Rügen (RGN, (d)), Sankelmark (SKMB, (e)) and Bad Segeberg (BSEG, (f)). The white dashed lines in (a) and (b) indicate the half peak wave period at locations P2 and P3 (for exact locations see Figure 3a, b). The black dashed lines show the half peak wave period at the FINO3 platform in the North Sea (for exact location see Figure 2a). BS: Baltic Sea, NS: North Sea, NA: North Atlantic.

2.1 Comparison of infrasound and seismic measurements

At large periods, acoustic waves in the atmosphere can travel long distances of up to several thousands of kilometres (e.g. De Groot-Hedlin et al. 2010). Infrasound describes the pressure fluctuations in a range between the acoustic cutoff frequency (3-10 mHz) and the lower human hearing frequency threshold of sound (generally 20 Hz). Infrasound enables us to investigate atmospheric noise during the October 2023 storm surge and its possible influence on the seismic data. It will provide indications that the sources of our seismic observations are transferred via the solid Earth or the atmosphere on a local scale. Continuous raw differential pressure data is processed the same way as the seismic data to investigate its spectral variations over time. Amplitude spectra are calculated over 15 min segments in a period range of 0.125−250 s and presented as spectrograms (Figure 6a and Figure S2 in the supplemental material). Further signal information can be derived using array processing on the different infrasound sensors of a station, here by applying the Progressive Multi-Channel Correlation (PMCC) method after Cansi (1995). This algorithm utilizes cross correlation functions to identify coherent infrasound events and their originating azimuth direction in several distinct period bands within 0.125−250 s. The IKUDE array processing features overall 8751 coherent detections between 18th and 29th October 2023, illustrated as a function of azimuth and number of detections (Figure 6b) or time (Figure S3), colour coded by their mean period, respectively.

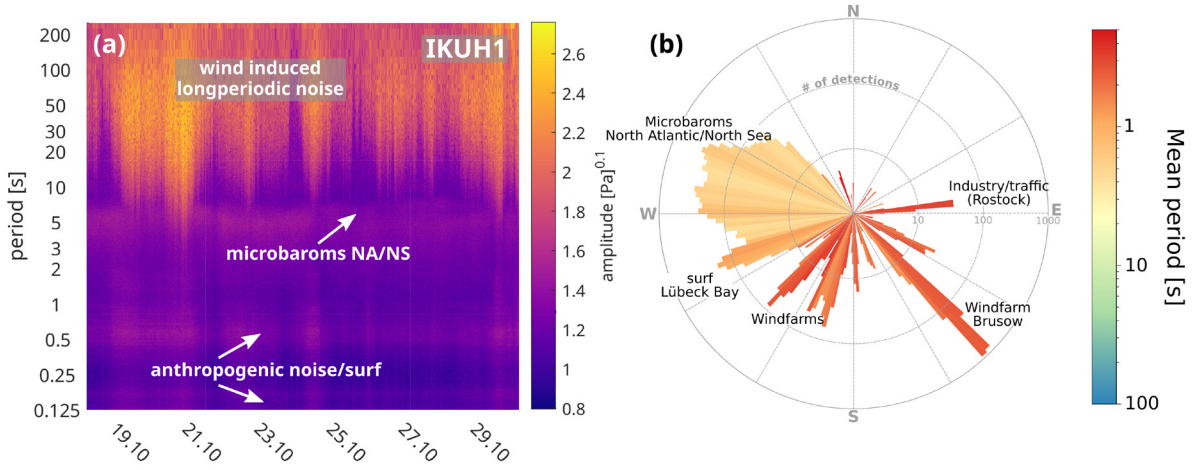

Figure 6: Infrasound measurements in Kühlungsborn during the storm surge event. The spectrogram of the infrasound station IKUH1 is shown on the left (a). The polar histogram (b) reveals the direction and number of infrasound detections during the same timeframe, colour coded by their mean period using the IKUDE infrasound network (for exact location see Figure 2d). NS: North Sea, NA: North Atlantic.

The spectrograms of all stations show highly similar results. They are dominated by large amplitudes at long periods of > 10 s on average. This long period noise is often related to large wind speeds (e.g. Matoza et al. 2009). During the October 2023 storm surge, large amplitudes are observed down to 5 s periods. However, no PMCC detection was registered for this period range which might be related to diffuse turbulences caused by varying wind speeds, generating only incoherent signals for which the array processing cannot derive consistent back azimuth directions. They show some similarities to long period seismic noise on the horizontal seismic component (Figure 4d) which needs further investigation. At around 5 s period, all infrasound spectrograms show a consistent band of increased

amplitudes over the entire time of investigation. They are related to microbaroms in the North Atlantic and probably the North Sea (Hupe et al. 2022, Kristoffersen et al. 2022). The polar-histogram confirms the source direction (Figure 6b). Detections with a mean period of around 5 s are originating from W-NW directions. Meanwhile, local microbaroms in the Baltic Sea are not observed. They might either be overprinted by the strong microbaroms from the North Atlantic and North Sea or subject to unfavourable propagation conditions. Infrasound propagation over long distances is generally dominated by ducting through semi-annually reversing stratospheric winds at around 50 kilometres altitude (Drob et al. 2003), which favour signals from western directions in winter months and from eastern directions during summer. The clear detectability of microbaroms from the west during the October 2023 storm surge may therefore explain reduced detection capabilities from E-NE directions (Baltic Sea), unless the sources were close (a few ten kilometres) and strong enough for detections following direct near-surface sound propagation.

Low period signals (< 1 s) are often related to anthropogenic sources, typically from sources at close distances. At periods < 2 s, there are several detections pointing in distinct directions from SE to SW. Most detections are measured during the October 2023 storm surge and later times (24th and 28th October) where the wind speed reaches maximum values, and can be attributed to local windfarms (Figure S3, e.g. Marcillo et al. 2015, Pilger and Ceranna 2017) at 3−13 km distance from the infrasound array. Easterly detections at the same periods might be related to traffic and industry in the nearby Port of Rostock. One cluster of detections is pointing in SW directions (≈240°−250°) with a mean period of ≈1 s. This might be due to surf (Le Pichon et al. 2010) in the Bay of Lübeck. The detections only occur at times of increasing wind speeds. However, they might be overprinted by the strong signals from the wind farms during other times (Figure S3). Comparison of seismic and infrasound data show very little correlation overall. Local secondary microseism of the Baltic Sea, measured in the period range of 1−3 s is not present in the infrasound data at comparable periods. Low period detections due to anthropogenic noise in the infrasound are not observed in the seismic spectrograms. Especially for the wind farms, the seismometers might be too distant to observe these low period signals. Possible reasons for that will be discussed in the next section. Potential surf related infrasound detections are also not observed in the seismic data. It might be difficult to distinguish them from secondary microseism of the Baltic Sea since they share a similar period range. Therefore, we conclude that ocean generated seismic waves rather propagate via the solid Earth than the atmosphere on a local scale.

3 Seismic monitoring of coastal regions

In the previous section, we observed a distinct decrease in secondary microseism amplitude of the Baltic Sea with increasing distance to the coast, whereas primary and secondary microseism amplitudes of the North Sea and North Atlantic are largely constant across all stations. In addition, we have shown that observations of ocean microseism are not contaminated by waves propagating through the atmosphere. To exploit seismic observations as a tool for monitoring of (near) coastal processes and suggest observational requirements for a potential seismic monitoring system in the Baltic Sea, we need to quantify this amplitude decrease. We calculate the mean seismic amplitude for each 15 min time window at periods between 1−3 s for each station (Figure 7a). Relative amplitudes (Figure 7b) are

estimated using the amplitudes of Kellenhusen as reference values, since it is closest to the coast. Distances for each station are given by their shortest distance to the coast (table in Figure 3c), from where we add the mean distance of the offshore local points P1, P2 and P3 to the coast line which is ≈5 km. The decrease in amplitude between the stations is especially distinct during the storm surge. Already at distances of ≈10 km, at near coastal sites, waveforms are damped by 20−40% but amplitudes also vary strongly over time. At larger distances of 25−40 km, amplitudes are at only 25−35% of the reference amplitudes from Kellenhusen.

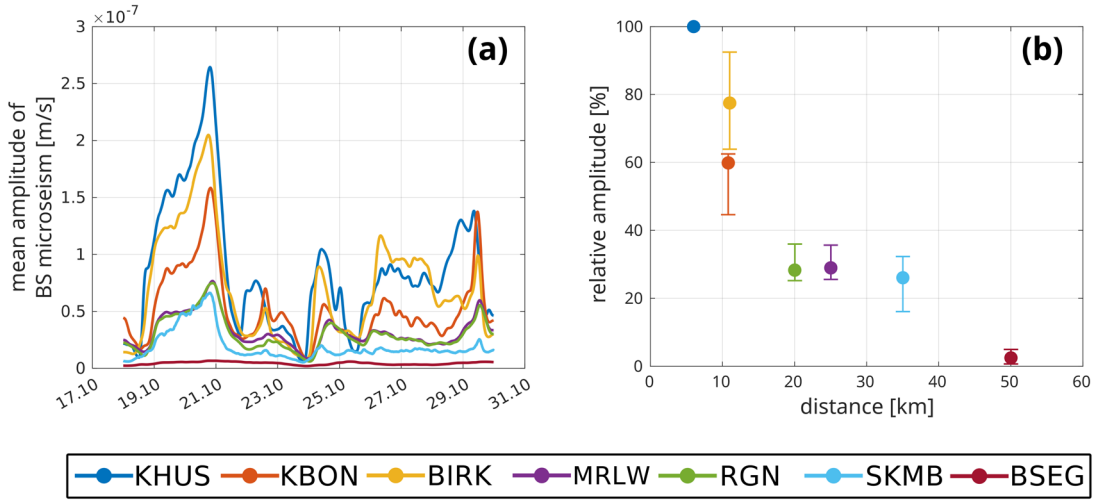

Figure 7: Mean amplitude of secondary microseism of the Baltic Sea of all stations along the Baltic Sea coast, extracted in a period range of 1–3 s (a). Their relative amplitude (b) is calculated using KHUS as reference station during the time of the storm surge. The coloured dots highlight the difference at the maximum amplitude of the October 2023 storm surge.

To derive a theoretical model of distance and period dependant damping of surface waves at the Baltic Sea coastal area, we use a relation for the amplitude of seismic surface waves, assuming the stationary phase approximation (after Dahlen and Tromp 1999):

$$A = \omega(cC)^{-1}\,(8\pi k|\sin(\Delta)|)^{-\frac{1}{2}}\left[\hat{r}U - i\hat{k}V + i\left(\hat{r}x\hat{k}\right)W\right]xR(\Phi)e^{i(s-1)\frac{\pi}{2}}e^{-\frac{\omega\Delta}{2CQ}} \quad (1)$$

where A is amplitude, c is phase velocity, C is group velocity, k represents the wave number, Q is the quality factor, $R(\Phi)$ indicates the radiation pattern, Δ is the distance, s is the wave group arrival index and ω is the angular frequency. The term $|sin(\Delta)|^{-1/2}$ represents the geometrical spreading, whereas $\hat{r}U - i\hat{k}V + i(\hat{r}x\hat{k})W$ defines the polarisation vector of a seismic surface wave. While the majority of the factors are not easily determined, the final one, $e^{-\frac{\omega\Delta}{2CQ}}$ is the anelastic damping, which we utilize to determine the amplitude damping of secondary microseism of the Baltic Sea as a function of distance to the coast and period. This reduces Eq. 1 to:

$$A = A_0 e^{-\frac{\omega\Delta}{2CQ}} \quad (2)$$

with A_0 as a reference amplitude, which we set to 1. We adapt a local model from the global compilation CRUST1.0 (Laske et al. 2013) with crustal seismic velocities and quality factors and modify it with a fast lower crustal layer and a crustal thickness of 30 km to comply with the general tectonic setting in Northern Germany (Figure 8a, Krawczyk et al. 2008). For

the uppermost crust, we use P-wave velocities from local borehole profiles provided by the Geological Survey Schleswig Holstein. As the quality factor decreases strongly in sedimentary layers compared to the crystalline crust, with values far below 100 (De Martin et al. 2021), we accordingly reduce Q_μ in the uppermost layers of the model. We use this model to calculate synthetic group velocity dispersion curves and quality factors as a function of period for Rayleigh and Love waves (Figure 8b), from which we derive the amplitude damping (Q) for Rayleigh (Figure 8c) and Love waves (Figure 8d) as a function of period and distance. Rayleigh waves are stronger damped at smallest periods compared to Love waves, whereas it is vice versa at large distances and longer periods. Surface waves of periods smaller than 3 s are already affected by damping at 10 km distance and are likely not detectable at distances larger than 40 km where their amplitude has decreased to < 50%, in line with our measurements. A precise detection of secondary microseism of the Baltic Sea is therefore starting to get difficult at stations which are more than ≈35 km from the coast. However, our estimations apply only for the time of the storm surge where amplitudes are amplified by large significant wave heights and maximum peak wave periods. Local detection capabilities might decrease to a maximum distance of < 25−30 km at times when there is no extreme weather event across the Baltic Sea. At the same time, seismic surface waves of periods > 8 s are almost unaffected by anelastic damping and can be therefore constantly measured over hundreds of kilometres, such as primary and secondary microseism from the North Atlantic and North Sea. The results also show that local wind parks in 3–3 km distance, which were detected by our infrasound measurements at periods < 1 s are also damped and therefore not measured by our seismometers.

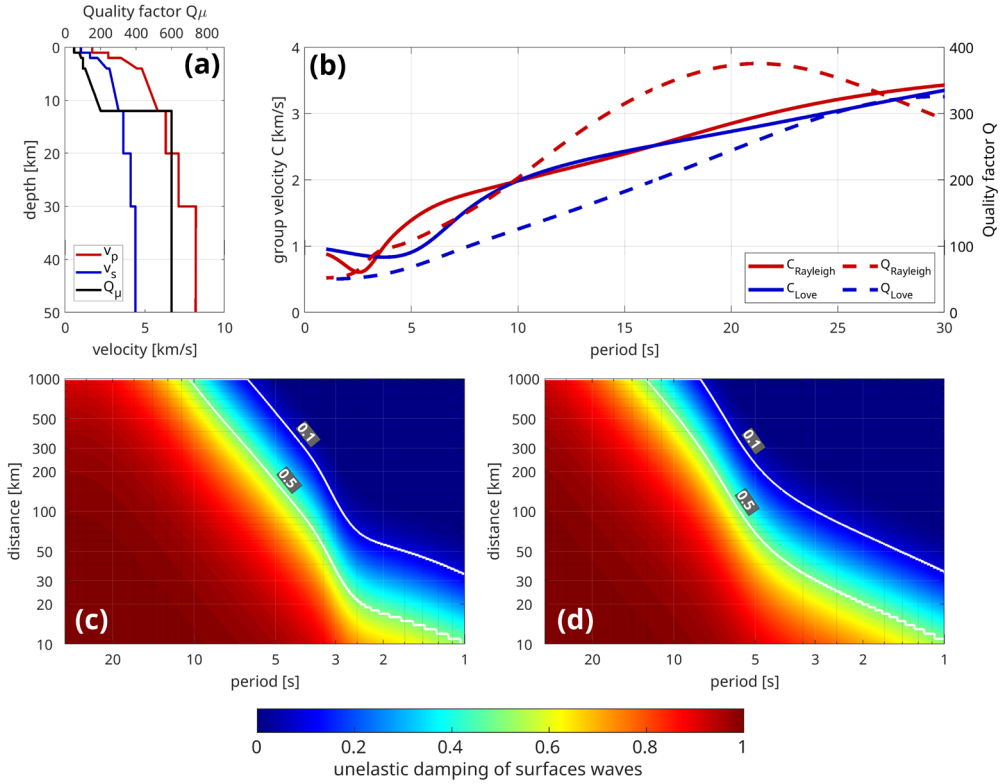

Figure 8: Modelling of anelastic damping of seismic surface waves using a local 1D model for P-wave velocity (v_p), S-wave velocity (v_s) and quality factor Q_μ of the subsurface (a). The 1D model is used to estimate synthetic group velocities (C) and quality factors (Q) as a function of period for Rayleigh and Love waves (b). This results in anelastic damping as function of distance and period for Rayleigh (c) and Love (d) waves.

4 Conclusion

We showed that seismic monitoring in coastal areas of the Baltic Sea, based on the expanded seismic network in northern Germany allows to investigate the effects of local weather and marine phenomena, such as the October 2023 storm surge on continuous seismic data. Seismic measurements show local variations at different sites along and with increasing distance to the Baltic Sea coast line. Near coastal stations in Kühlungsborn, Birkenmoor and Kellenhusen reveal locally variable secondary microseism of the Baltic Sea which correlate with the half peak wave periods of ocean surface gravity waves at nearby offshore locations. Infrasound measurements in Kühlungsborn reveal additional insight on noise sources and atmospheric wave propagation. Low period signals are related to wind farms and occasionally surf which were detected during the October 2023 storm surge event and correspond in general to increased wind speeds. However, we find that infrasound and seismic data do not generally correlate. This indicates that the observed seismic signals are most likely not directly related to atmospheric sources, but propagate through the solid Earth when induced by ocean generated microseism. Finally, our seismic measurements enable us to estimate a sensitivity range for local microseism in coastal areas of the Baltic Sea using a synthetic approach for anelastic damping as a function of period and distance to the coast. As a result, seismic monitoring of locally generated ocean microseism in coastal areas along the Baltic Sea would be possible within 25−30 km distance to coast.

4.1 Data availability statement

Seismic waveform and infrasound data from the German Regional Seismic Network (GR; https://doi.org/10.25928/mbx6-hr74), GEOFON (GE; https://doi.org/10.14470/TR560404) and Kiel University Earthquake Monitoring (KQ; https://doi.org/10.7914/SN/KQ) can be obtained from the GEOFON data centre of the German Research Centre for Geoscience (GFZ; https://geofon.gfz-potsdam.de/). Sea state data of the FINO3 platform used in this study can be obtained from the Sea State portal of the Federal Maritime and Hydrographic Agency (BSH; https://seastate.bsh.de/rave/index.jsf?content=seegang). Water level data can be obtained from the ITZBund and the Federal Waterways and Shipping Administration (WSV, pegelonline.wsv.de). Modelled Sea state data of the Baltic Sea is provided by the Norwegian Meteorological Institute (MET) and can be obtained from the Copernicus Marine Environment Monitoring Service (CMEMS; https://doi.org/10.48670/moi-00002). Weather data is used from the Open Data Server of the German Meteorological Service (DWD; https:// opendata.dwd.de/climate_environment/CDC/observations_germany/climate/10_ minutes/wind/recent/).

5 References

Ardhuin, F.; Stutzmann, E.; Schimmel, M.; Mangeney, A.: Ocean wave sources of seismic noise. In: Journal of Geophysical Research: Oceans, 116 (C9), 2011.

Ardhuin, F.; Balanche, A.; Stutzmann, E.; Obrebski, M.: From seismic noise to oceanwave parameters: General methods and validation. In: Journal of Geophysical Research: Oceans, 117 (C5), 2012.

Ardhuin, F.; Gualtieri, L.; Stutzmann, E.: How ocean waves rock the earth: Two mechanisms explain microseisms with periods 3 to 300 s. In: Geophysical Research Letters, 42(3), 765–772, 2015.

Ardhuin, F.; Sutherland, P.; Doble, M.; Wadhams, P.: Ocean waves across the arctic: Attenuation due to dissipation dominates over scattering for periods longer than 19 s. In: Geophysical Research Letters, 43(11), 5775–5783, 2016.

Becker, D.; Cristiano, L.; Peikert, J.; Kruse, T.; Dethof, F.; Hadziioannou, C.; Meier, T.: Temporal modulation of the local microseism in the North Sea. In: Journal of Geophysical Research: Solid Earth, 125(10), e2020JB019770, 2020.

Bertelli, T.: Osservazioni sui piccoli movimenti dei pendoli in relazione ad alcuni fenomeni meteorologici del pd timoteo bertelli barnabita. Tip. delle scienze matematiche e fisiche, 1872.

Bretschneider, C. L.: Wave variability and wave spectra for wind-generated gravity waves (No. 118). The Board, 1959.

Bromirski, P. D.; Duennebier, F. K.: The near-coastal microseism spectrum: Spatial and temporal wave climate relationships. In: Journal of Geophysical Research: Solid Earth, 107(B8), ESE–5, 2002.

BSH: Schwere Sturmflut vom 20. Oktober 2023. Retrieved 22.07.2024, from https://www.bsh.de/DE/THEMEN/Wasserstand_und_Gezeiten/ Sturmfluten_Anlagen/Downloads/Ostsee_Sturmflut_20231020.pdf?__blob= publicationFile&v=3, 2024.

Cansi, Y.: An automatic seismic event processing for detection and location: The pmcc method. In: Geophysical research letters, 22(9), 1021–1024, 1995.

Cutroneo, L.; Ferretti, G.; Barani, S.; Scafidi, D.; De Leo, F.; Besio, G.; Capello, M.: Near real-time monitoring of significant sea wave height through microseism recordings: Analysis of an exceptional sea storm event. In: Journal of Marine Science and Engineering, 9(3), 319, 2021.

Davy, C.; Barruol, G.; Fontaine, F. R.; Sigloch, K.; Stutzmann, E.: Tracking major storms from microseismic and hydroacoustic observations on the seafloor. In: Geophysical Research Letters, 41(24), 8825-8831, 2014.

Dahlen, F. A.; Tromp, J.: Theoretical Global Seismology. In: Physics Today, 52, 418-419. DOI: 10.1063/1.882788, 1999.

Deacon, G. E. R.: Relations between sea waves and microseisms. In: Nature, 160(4065), 419–421, 1947.

De Groot-Hedlin, C. D.; Hedlin, M. A.; Drob, D. P.: Atmospheric variability and infrasound monitoring. Infrasound monitoring for atmospheric studies, 475-507, 2009.

De Martin, F.; Chaljub, E.; Thierry, P.; Sochala, P.; Dupros, F.; Maufroy, E.; Hadri, B.; Benaichouche, A.; Hollender, F.: Influential parameters on 3-d synthetic ground motions in a sedimentary basin derived from global sensitivity analysis. In: Geophysical Journal International, 227(3), 1795–1817, 2021.

Drob, D. P.; Picone, J. M.; Garce´s, M. A.: Global morphology of infrasound propagation. In: Journal of Geophysical Research: Atmospheres, 108(D21), 2003.

Essen, H.-H.; Krüger, F.; Dahm, T.; Grevemeyer, I.: On the generation of secondary microseisms observed in northern and central europe. In: Journal of Geophysical Research: Solid Earth, 108(B10), 2003.

Ferretti, G.; Barani, S.; Scafidi, D.; Capello, M.; Cutroneo, L.; Vagge, G.; Besio, G.: Near real-time monitoring of significant sea wave height through microseism recordings: An application in the Ligurian Sea (Italy). In: Ocean & Coastal Management, 165, 185-194, 2018.

Hupe, P.; Ceranna, L.; Le Pichon, A.; Matoza, R. S.; Mialle, P.: International monitoring system infrasound data products for atmospheric studies and civilian applications. In: Earth System Science Data Discussions, 1–40, 2022.

Iafolla, L.; Fiorenza, E.; Chiappini, M.; Carmisciano, C.; Iafolla, V. A.: Sea wave data reconstruction using micro-seismic measurements and machine learning methods. In: Frontiers in Marine Science, 9, 798167, 2022.

Juretzek, C.; Hadziioannou, C.: Where do ocean microseisms come from? a study of love-to-rayleigh wave ratios. In: Journal of Geophysical Research: Solid Earth, 121(9), 6741–6756, 2016.

Juretzek, C.; Hadziioannou, C.: Linking source region and ocean wave parameters with the observed primary microseismic noise. In: Geophysical Journal International, 211(3), 1640-1654, 2017.

Krawczyk, C.; Rabbel, W.; Willert, S.; Hese, F.; Götze, H.-J.; Gajewski, D.; et al.: Crustal structures and properties in the cebs from geophysical evidence. In: Dynamics of complex intracontinental basins: The central european basin system, 67–95, 2008.

Kristoffersen, S. K.; Le Pichon, A.; Hupe, P.; Matoza, R. S.: Updated global reference models of broadband coherent infrasound signals for atmospheric studies and civilian applications. In: Earth and Space Science, 9(7), e2022EA002222, 2022.

Laske, G.; Masters, G.; Ma, Z.; Pasyanos, M.: Update on crust1. 0—a 1-degree global model of earth's crust. In: Geophysical research abstracts, 15, 2658, 2013.

Le Pichon, A.; Matoza, R.; Brachet, N.; Cansi, Y.: Recent enhancements of the pmcc infrasound signal detector. In: Inframatics, 26, 5–8, 2010.

Lepore, S.; Grad, M.: Analysis of the primary and secondary microseisms in the wavefield of the ambient noise recorded in northern poland. In: Acta Geophysica, 66, 915–929, 2018.

Leydecker, G.: Erdbebenkatalog für Deutschland mit Randgebieten für die Jahre 800 bis 2008, 2011.

Longuet-Higgins, M. S.: A theory of the origin of microseisms. Philosophical Transactions of the Royal Society of London. In: Series A, Mathematical and Physical Sciences, 243(857), 1–35, 1950.

Marcillo, O.; Arrowsmith, S.; Blom, P.; Jones, K.: On infrasound generated by wind farms and its propagation in low-altitude tropospheric waveguides. In: Journal of geophysical research: Atmospheres, 120(19), 9855–9868, 2015.

Matoza, R. S.; Garcés, M. A.; Chouet, B. A.; D'Auria, L.; Hedlin, M. A.; De Groot-Hedlin, C.; Waite, G. P.: The source of infrasound associated with long-period events at mount st. helens. In: Journal of Geophysical Research: Solid Earth, 114(B4), 2009.

Moschella, S.; Cannata, A.; Cannavò, F.; Di Grazia, G.; Nardone, G.; Orasi, A.; Picone, M.; Ferla, M.; Gresta, S.: Insights into microseism sources by array and machine learning techniques: Ionian and Tyrrhenian Sea case of study. In: Frontiers in Earth Science, 8, 114, 2020.

Omori, F.: Horizontal pendulums for the mechanical registration of seismic and other earth movements. In: The journal of the College of Science, Imperial University of Tokyo, Japan, 11(3), 121–145, 1899.

Pierson Jr, W. J.; Moskowitz, L.: A proposed spectral form for fully developed wind seas based on the similarity theory of sa kitaigorodskii. In: Journal of geophysical research, 69(24), 5181–5190, 1964.

Pilger, C.; Ceranna, L.: The influence of periodic wind turbine noise on infrasound array measurements. In: Journal of Sound and Vibration, 388, 188–200, 2017.

Stammler, K.; Bischoff, M.; Brüstle, A.; Ceranna, L.; Donner, S.; Fischer, K.; Gaebler, P.; Friederich, W.; Funke, S.; Hartmann, G.; Homuth, B.; Knapmeyer-Endrun, B.; Korn, M.; Megies, T.; Pilger, P.; Plenfisch, T.; Pustal, I.; Rappsilber, I.; Schmidt, B.; Sonnabend, L.; Stange, S.; Wasserman, J.; Wegler, U.: German seismic and infrasound networks contributing to the European integrated data archive (EIDA). In: Seismological Research Letters, 92(3), 1854-1875, 2021.

Webb, S. C.: Broadband seismology and noise under the ocean. In: Reviews of Geophysics, 36(1), 105-142, 1998.

Webb, S. C.; Crawford, W. C.: Shallow-water broadband OBS seismology. In: Bulletin of the Seismological Society of America, 100(4), 1770-1778, 2010.

Wiechert, E.: Verhandlungen der zweiten internationalen seismologischen konferenz. In: Gerlands Beitr. Geophys, 2, 41–43, 1904.

Zöppritz, K.: Seismische registrierungen in göttingen im jahre 1906. In: Nachrichten von der Gesellschaft der Wissenschaften zu Göttingen, Mathematisch-Physikalische Klasse, 1908, 129–190, 1908.

6 Supplemental Material

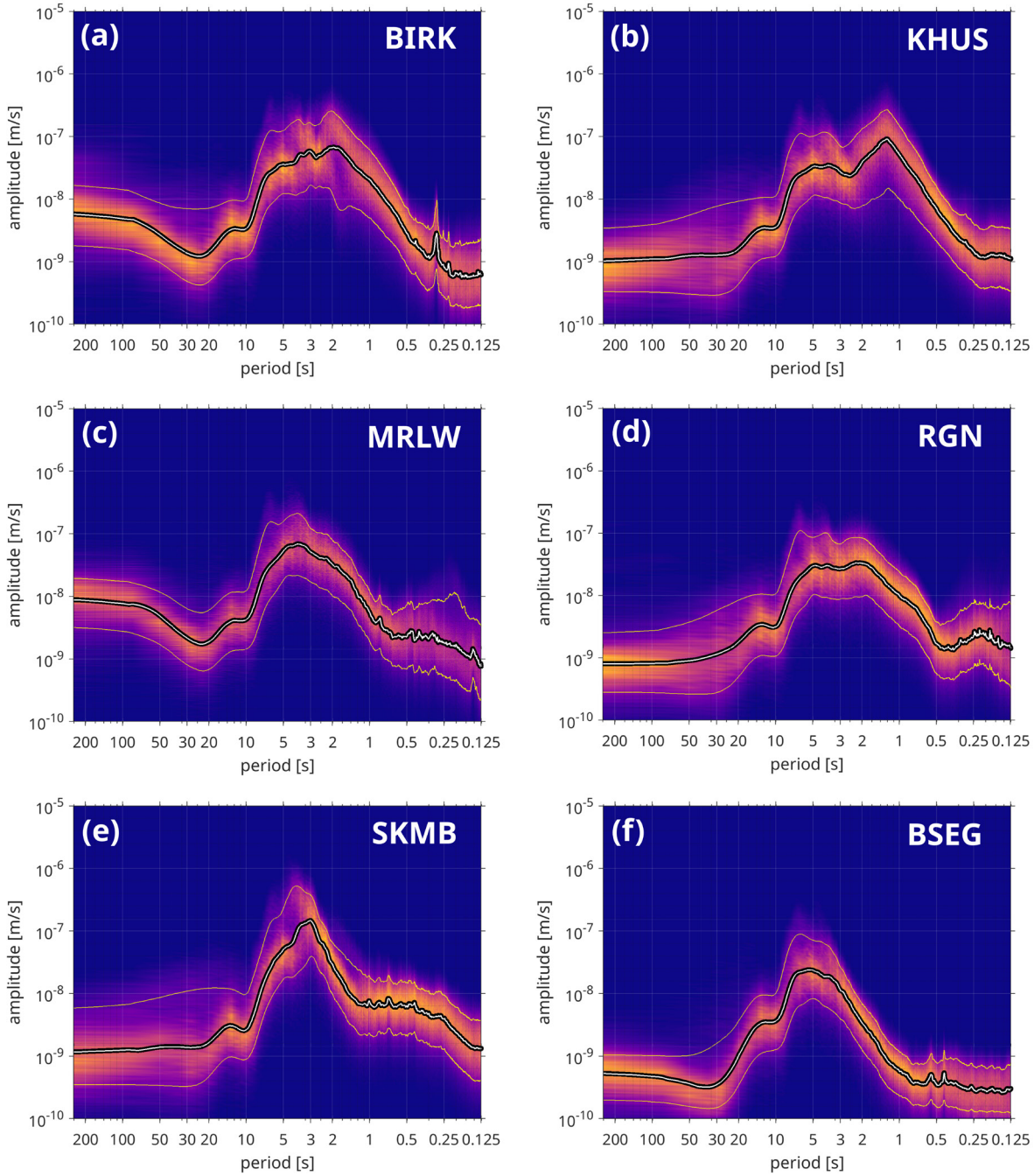

Figure S1: Histograms of vertical component amplitude spectra for the seismic stations Birkenmoor (a), Kellenhusen (b), Marlow (c), Rügen (d), Sankelmark (e) and Bad Segeberg (f) in a period band of 0.125 to 250 s. The median amplitude (white line) and the 10 and 90 percent percentiles (yellow lines) are highlighted.

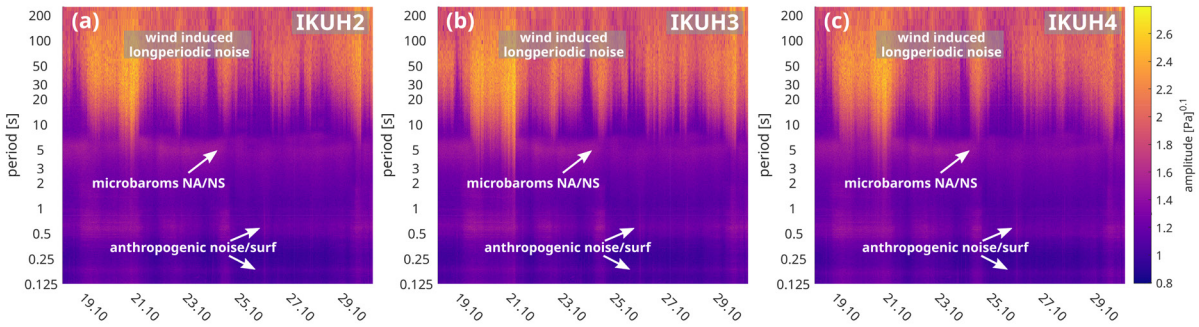

Figure S2: Spectrograms of infrasound data from stations IKUH2 (a), IKUH3 (b) and IKUH4 (c). NS: North Sea, NA: North Atlantic.

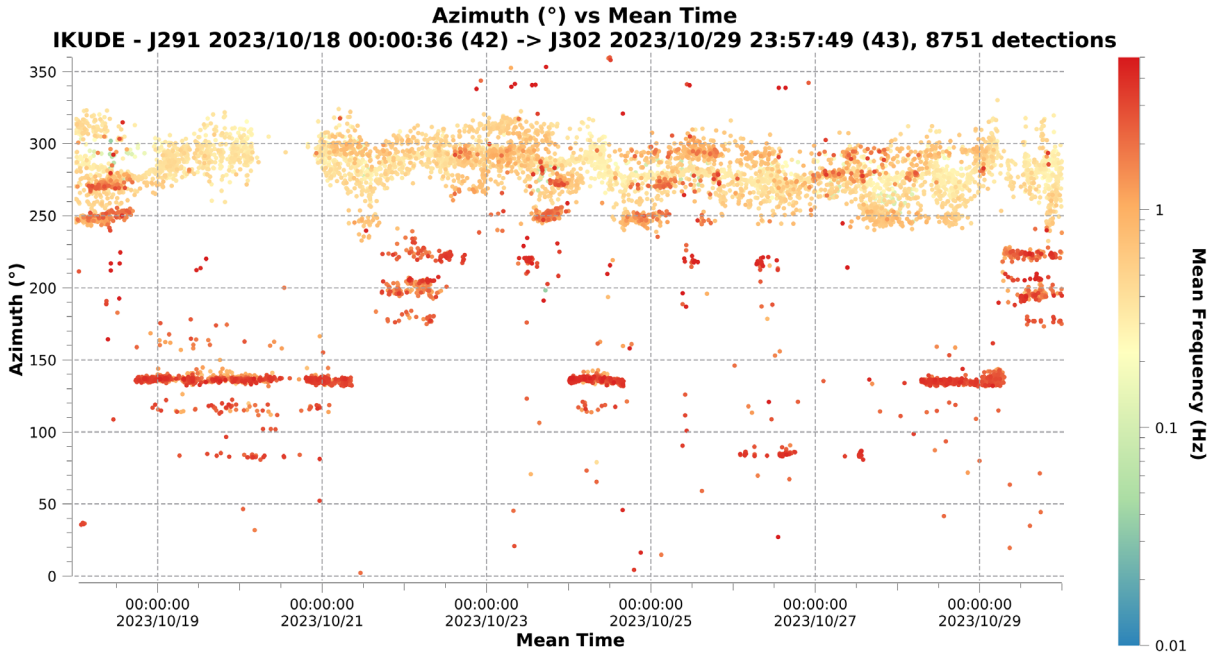

Figure S3: Infrasound detections as function of azimuth from 18th to 29th October. The 8751 detections are colour-coded by mean frequency in a range between 0.01 and 4 Hz.